JMEPEG (2021) 30:1748–1758
https://doi.org/10.1007/s11665-021-05476-y

1059-9495/$19.00

Synthesis and Characterization of Ti6Al4V-Nano-ZrO_2 Composite Cladding on Ti6Al4V Substrate Using Fiber Laser

Anand M. Murmu, S.K. Parida, and A.K. Das

Submitted: 4 August 2020 / Revised: 14 December 2020 / Accepted: 7 January 2021 / Published online: 27 January 2021

The synthesis and characterization of Ti6Al4V-nano-ZrO_2 composite coatings on Ti6Al4V substrate using laser cladding method have been carried out. The effect of laser power and scanning speed on the clad layer morphology, microhardness, phase appearance, and tribological behavior of the composite cladding has been investigated. The formation of dendrite microstructure with retention of agglomerated nano-ZrO_2 powder and metallic oxides such as TiO_2, Al_2O_3, ZrO_2 increases hardness and wear resistance of the cladding surface remarkably. The average microhardness of the cladding surface increased 4 times that of the substrate material. The discontinuous but uniformly dispersed reinforcement of ZrO_2 is formed during the melting and solidification process. Cracks and pores and discontinuous phases of ZrO_2 are also found in some of the samples. These discontinuous sites can retain lubricant; hence, the tribological behavior of the laser cladding composite coating may improve. This method establishes the reactive in situ formation of hard composite coating (TiO_2-Al_2O_3-ZrO_2) with a lower coefficient of friction than the Ti6Al4V using laser irradiation of wavelength 1070 nm.

Keywords cladding, composite, laser energy density, reinforcement, synthesis, titania, zirconia

1. Introduction

Titanium alloy (Ti6Al4V) is widely used in aerospace, biomedical, chemical, and seawater-desalination industries due to its high specific strength and excellent corrosion resistance. Its high-temperature oxidation and wear resistance can further be improved by depositing a thermal barrier overlay coating using several surface engineering techniques. Some of the earlier overlay coating methods on Ti6Al4V alloys were by Zhou et al. (Ref 1), Koshuro et al. (Ref 2), Selivanov et al. (Ref 3), Wiecinski et al. (Ref 4), Sitek et al. (Ref 5), Xu and Shen (Ref 6), etc. Zhou et al. (Ref 1) proposed an air plasma-sprayed YSZ overlay coating method with major retention of tetragonal zirconia on Ti6Al4V alloy for high-temperature application. They reported that increasing the layer thickness reduces the adhesion strength of the YSZ coating on Ti6Al4V substrate. Koshuro et al. (Ref 2) deposited plasma-sprayed Al_2O_3 on Ti6Al4V alloy to improve its wear properties. They observed the in situ formation of TiO_2-Al_2O_3 resulted in a porous coating that could reduce the porosity by subsequently processing it by micro-arc oxidation method. Selivanov et al. (Ref 3) investigated the effect of layering sequence, and layer thickness of a PVD-coated TiN, Ti-Al-N on Ti6Al4V alloy on the interlayer stresses to avoid delamination. Similarly, Wiecinski et al. (Ref 4) studied the effect of layering sequence and material properties of individual layers of sputtered (PVD) metal/ceramic and ceramic/ceramic multilayer coatings on titanium alloy on the microhardness and elastic modulus. Sitek et al. (Ref 5) chemically deposited Ti-Al-N phases on Ti6Al4V alloy to improve its abrasive wear resistance. They suggested subsequent heat treatment can improve the adhesion strength of the coating layer as well as its microhardness. Xu and Shen (Ref 6) could improve the hardness and wear resistance properties of pure Ti by deposition of TiO_2/nano-SiO_2 using the micro-arc oxidation method. However, using laser energy one can quickly produce a very dense functional coating with tailor-made properties with a suitable choice of laser source parameters. Several attempts have been made by many researchers to improve the surface properties of Ti6Al4V alloy by laser cladding of ceramics, carbide, and nitride. Obadele et al. (Ref 7) studied the effect of zirconia (ZrO_2) addition in the TiNi metal matrix composite on Ti6Al4V substrate using laser cladding method and reported the reduction in coefficient of friction. The improvement in chemical resistance properties of Ti6Al4V alloy, by alloying zirconium in it, has been reported by Xia et al. (Ref 8). Liu et al. (Ref 9) could produce a lubricious AlSi10Mg coating on Ti6Al4V substrate using laser energy. Kumar et al. (Ref 10) investigated about the wear resistance of (AlN + Ni + Ti6Al4V) composite coating on Ti6Al4V alloy produced by laser cladding and reported approximately three times higher hardness of the coating than the substrate. In recent years, zirconium dioxide (ZrO_2) has become a suitable choice of material because of its high strength and hardness, high melting point, better chemical stability, thermal barrier capability, high wear, and corrosion resistance. Lepule et al. (Ref 11) experimentally demonstrated the effects of ZrO_2 on the corrosion and wear behavior of NiTi-ZrO_2 coatings on AISI 316 stainless steel processed by a laser deposition technique. Ma et al. (Ref 12) could produce dense yttria-

Anand M. Murmu and **S.K. Parida**, National Institute of Foundry and Forge Technology, Ranchi, Jharkhand 834003, India; and **A.K. Das**, Indian Institute of Technology (ISM) Dhanbad, Dhanbad, Jharkhand 826004, India. Contact e-mails: anand.murmu@gmail.com, sambitparida@gmail.com, and eralok@yahoo.co.in.

stabilized zirconia (YSZ) coating on titanium alloy using the ultrasonic-assisted laser cladding technique to improve its wear resistance. As per Isao and Masayuki (Ref 13), direct melting of the zirconia (refractive index of 2.23) alone is difficult using fiber laser (wavelength 1076 nm) as it transmits and reflects (more than 70 and 20%, respectively) the laser irradiation. Wilkes et al. (Ref 14) reported that the cladding of ZrO_2 through laser melting alone may form cracks due to rapid solidification. Hattal et al. (Ref 15) reported that sound parts with higher strength and hardness can be manufactured using a metallic powder of Ti6Al4V with the addition of nano-YSZ 2.5% by selective laser melting (SLM). However, the cladding of ZrO_2-Ti6Al4V preplaced powder with higher weight percentage of ZrO_2 has not been reported so far.

The motive of this research is to improve the wear resistance of Ti6Al4V substrate with preplaced powder of ZrO_2 mechanically mixed with Ti6Al4V powder in various proportions and also to investigate the effect of process parameters such as laser power, scanning speed, gas flow rate on the microstructure, cladding thickness, hardness, appearance of defects and wear properties of the resulting deposition for getting sound cladding of ZrO_2 on Ti6AL4V substrate using a fiber laser. In addition to it, in this method, one can obtain a coating containing a mixture of Al_2O_3, TiO_2, and ZrO_2 in situ reactively in a single process at once. Schaedler et al. (Ref 16) reported that the formation of TiO_2 is advantageous for the composite cladding TiO_2-ZrO_2 as it will help to stop tetragonal to the monoclinic transformation of ZrO_2 during solidification. Moreover, the solution of TiO_2 and ZrO_2 will enhance the toughness of the resulted cladding.

2. Materials and Methods

A 400 W continuous-wave fiber laser with a central emission wavelength of 1070 nm (SM-S00051, SPI fiber) is used for producing a composite coating on the Ti6Al4V substrate. The scanning pattern of the cladding was controlled by the precise movement of the specimen fixed on the 3-axis CNC controlled table. A 5-mm-thick Ti6Al4V (grade 5 alloy) plate was selected as substrate material. Its top surface was roughened using 1000 grit size SiC emery paper for good adhesion of the premixed composite powder paste. A weighed quantity of the Ti6Al4Vand nano-ZrO_2 powders was mixed for 30 min in a grinding bowl to prepare a homogeneous mixture. Thoroughly mixing by hand pressure encapsulate the zirconia powder with Ti6Al4V powder and mechanically stick no its surface, thus reducing its transparency and reflectivity to the laser beam. This may help in melting ZrO_2 without reflecting and transmitting much of the laser energy incident on them. The powder mixtures were prepared in 60-40, 70-30, 75-25, 80-20 percentage by weight of Ti6Al4V and ZrO_2, separately. The mixed powder paste was prepared using polyvinyl alcohol (PVA) as a binder and applied to the substrate surface. Uniform paste thickness of 1 mm was maintained with the help of a rectangular glass plate and zirconia balls of 1 mm diameter, and then, it was kept inside the oven at 60 °C for 12 h to remove moisture before exposing it to laser irradiation. FESEM images of the nano-ZrO_2 powders used in the experiments are shown in Fig. 1. Several experiments were conducted with a varying weight percentage of Ti6Al4V and nano-ZrO_2 powders with various laser energy density and scanning speed. Figure 2

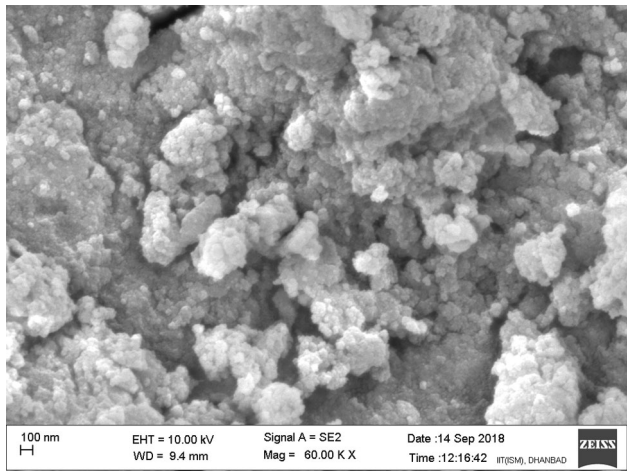

Fig. 1 FESEM image of nano-ZrO_2powders

shows the typical cross-sectional micrographs of the cladded samples done by varying the weight percentage of Ti6Al4V:ZrO_2 (60:40) (Fig. 2a), 70:30 (Fig. 2b), 75:25 (Fig. 2c), 80:20 (Fig. 2d) cladded with a laser energy density of 45 J/mm^2. More cracks and pores are observed with a higher weight percentage of the ZrO_2 (Fig. 2a, b), whereas smaller cracks and pores are observed in the cladded samples prepared with 75:25 weight percentage of Ti6Al4V:ZrO_2 (Fig. 2c). No cracks and pores are observed in the sample prepared with 80:20 weight percentage of Ti6Al4V:ZrO_2 cladded with a laser energy density of 45 J/mm^2. From these experiments, Ti6Al4V (80 wt.%) and ZrO_2 (20 wt.%) were selected as a suitable mixture for making composite powder for cladding. This phenomenon was observed in almost all the claddings irrespective of laser energy. With a relatively low weight percentage of ZrO_2, the hardness and wear properties approach that of the base metal; hence, Ti6Al4V:ZrO_2 (80:20) is continued for the rest of the experiments. Moreover, as reported by Schaedler et al. (Ref 16), 80 molar percentage of TiO_2 and 20 molar percentage of ZrO_2 forms eutectic composition which has a minimum melting point temperature. The experiments were conducted with a combination of several process parameters as shown in Table 1. During the cladding, a 1 mm distance between the scanning paths of the laser beam was maintained to ensure 50% overlapping of claddings. The cladding samples were allowed to cool in an open environment. The powder morphology, cladding thickness, and microstructure were examined using an optical microscope (Olympus, BH2-UMA), FESEM Supra 55, and SEM (EVO 18, Carl Zeiss, UK) equipped with EDS detector, make Bruker Xflash 6130, Germany. Dendritic arm spacing (DAS) analysis of the microstructure was conducted using Olympus, BH2-UMA Stream Basic software. Microhardness testing was performed using a Vickers microhardness-testing machine (BHT 1000) with a test load of 1 kg and a dwelling time of 10 s. Phase analysis was carried out using an x-ray diffractometer (SmartLab diffractometer, Rigaku). Wear test was performed using a pin-on-disk wear testing machine (DUCOM, TR 20-LE-M5) as per the ASTM G99. The wear test parameters are shown in Table 2. Further, the elemental analysis was performed using x-ray photoelectron spectroscopy (XPS, PHI 5000 Versa Probe III, Japan).

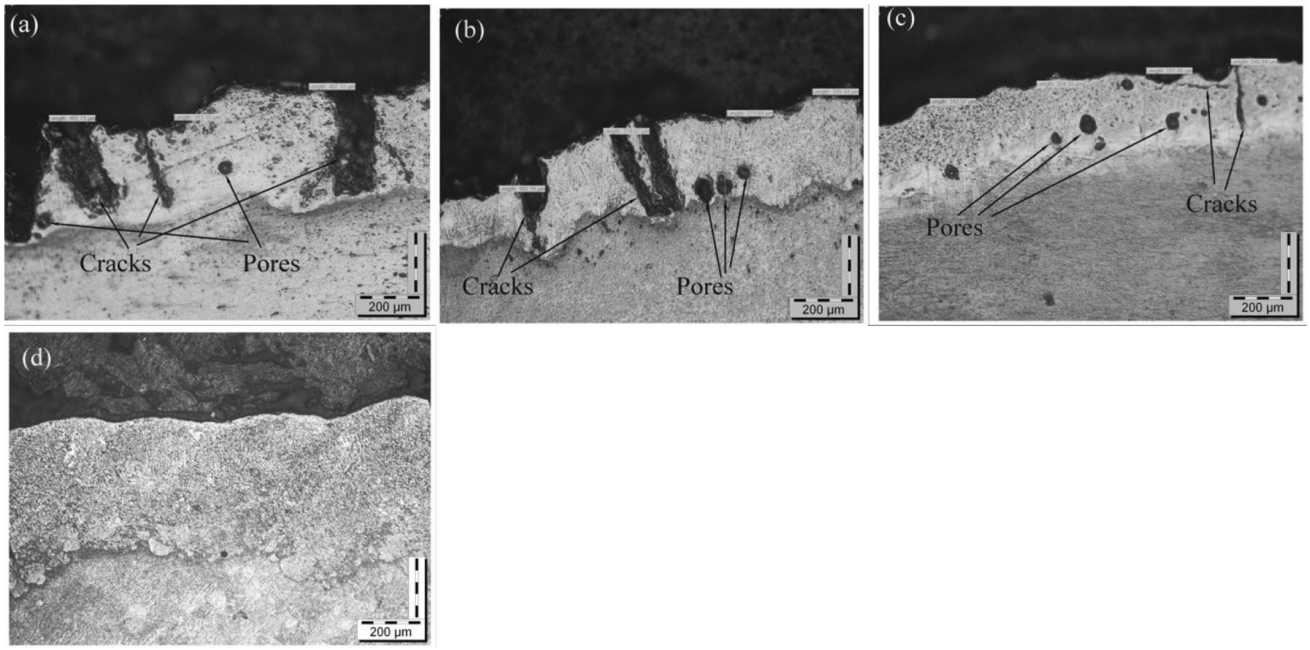

Fig. 2 Cross-sectional micrographs with the variation of weight percentage of ZrO_2in the cladding (a) Ti6Al4V:ZrO_2 (65:35); (b) Ti6Al4V:ZrO_2 (70:30); and (c)Ti6Al4V:ZrO_2 (75:25); (d) Ti6Al4V:ZrO_2(80:20)

Table 1 Details of material and process parameters

Material properties		Process parameters	
Substrate material	Ti6Al4V, Grade-5	Laser power, W	150, 200, 250
Hardness	350-370 HV	Scanning speed, m/min	200, 400, 600
Melting point	1878-1933 K	The thickness of the substrate, mm	5
		Binder	Polyvinyl alcohol
		Preplaced powder paste: height, mm	1
		Beam type	Continuous-wave
		Spot diameter, mm	1

Table 2 Details of wear test parameters

Load, kg	20, 30, 40 N
Speed, RPM	700
Distance, km	1, 2, 3

3. Results and Discussions

3.1 Morphological and Microstructure Study of the Laser Cladding Composite Coatings

In this section, the variation in cladding thickness, change in microstructure due to melting and solidification, and appearance of micropores, cracks with the variation of laser energy density have been analyzed from the cross-sectional images.

3.1.1 Clad Layer Thickness. The cladding layer thickness and its morphology are significantly affected by the magnitude of incident laser energy density. The optical micrographs of the cross section of the cladded samples prepared (manually hand pressure mixed) and preplaced powder of Ti6Al4V (80):ZrO_2 (20) weight percentage incident by laser energy density 15, 22.5, 30, 45, 60, 75 J/mm^2 are shown in Fig. 3(a), (b), (c), (d), (e) and (f), respectively. At low laser energy input (15-30 J/mm^2), partial melting and solidification of composite powder have taken place during the cladding process, which influences the strength and the thickness of the clad material (Fig. 3a–c). At higher values of laser energy input (45, 60, 75 J/mm^2), a higher amount of composite powder melting (Fig. 3d–f) has taken place which resulted in increasing the cladding thickness. The columnar dendritic structure appears in samples prepared at 30, 45, 60, 75 J/mm^2 laser energy (Fig. 3c–f). The length of the dendrites appears to grow in size when the laser energy density is increased beyond 30 J/mm^2. The interdendritic space is minimum at the laser energy density 45 J/mm^2 (Fig. 3d). It is maximum in the samples prepared at the laser energy density of 75 J/mm^2. This may be due to the evaporation of composite powder at this level of laser energy density resulting in higher interdendritic space than other samples. A similar observation has been found in the plots representing the variation of the average cladding thickness with laser energy density (Fig. 4).

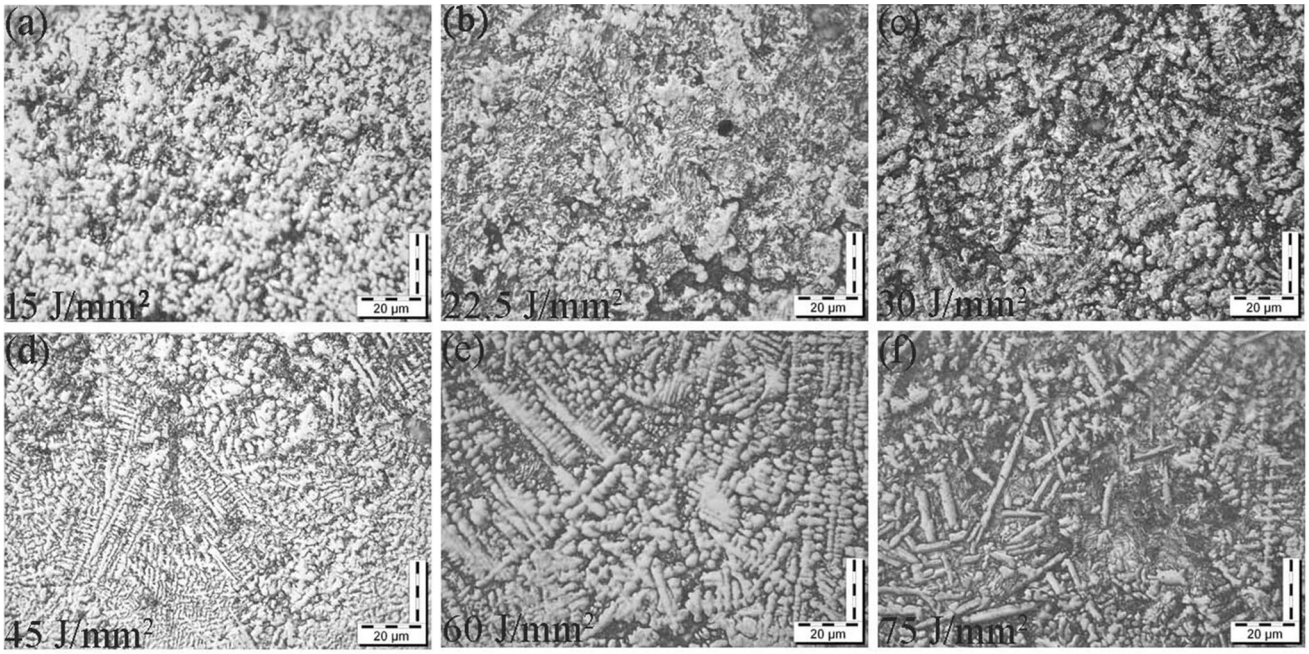

Fig. 3 Optical micrographs of the cross section of composite coatings [Ti6Al4V (80):ZrO_2 (20) weight percentage] samples done by irradiating laser energy density (a) 15 J/mm^2, (b) 22.5 (c) 30 J/mm^2, (d) 45 J/mm^2, (e) 60 J/mm^2, (f) 75 J/mm^2

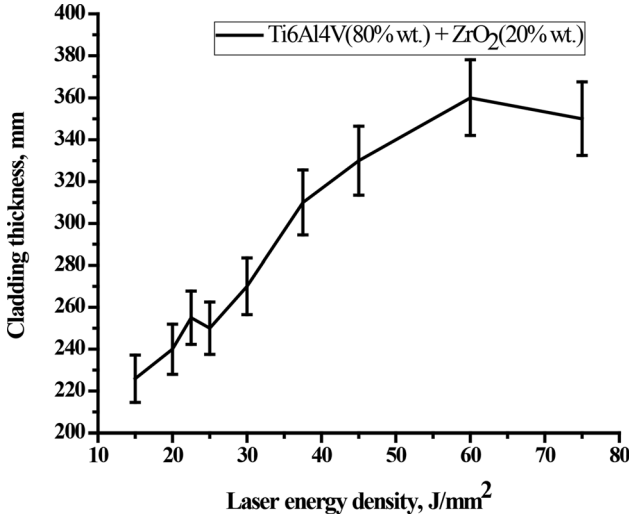

Fig. 4 Variation of cladding thickness with laser energy density

The average clad layer thickness increases with increasing the laser energy density up to 60 J/mm^2, and thereafter, it reduces with a further increase in laser energy density (Fig. 4). This can also be seen from the SEM images (Fig. 5a–d) showing the clad thickness with variation laser energy density of 37.5, 45, 60, 75 J/mm^2, respectively. But, beyond 60 J/mm^2, the cladding thickness reduces due to the accumulation of excess energy in a point at a particular instant causing direct evaporation of preplaced powder. A similar investigation has been reported by Chakraborty et al. (Ref 17). The grain sizes are smaller in the samples prepared at 45 J/mm^2 with a denser distribution of the grains. Some retained nano-ZrO_2 powder is found in Fig. 5(b) and (c). The defects like micro-cracks and pores are also observed in the claddings (Fig. 5a, b). But no horizontal cracks are observed in any of the composite cladding. Horizontal cracks are more vulnerable to peeling up of the coating than vertical cracks. The vertical cracks appeared because of the difference in the thermo-physical property of elements and compounds. The cladding appears as dense and smooth zones, indicating the good molten state of particles (Fig. 5a–c), whereas in Fig. 3(d) the cladding appears to be less dense due to evaporation and higher dilution of ZrO_2 at a laser energy density of 75 J/mm^2. The dendritic length and interdendritic space depend on the cooling rate and energy input. The average dendritic length is found to be 8, 11, 12, 18.73, 21.7 μm with the laser energy input of 30, 37.5, 45, 60, 75 J/mm^2, respectively. However, the interdendritic space decreases from 4, 2.61, 1.84 μm for a laser energy input of 30, 37.5, 45 J/mm^2, and thereafter, it further increases. This increase in interdendritic space at higher laser energy input (i.e., 75 J/mm^2) is due to localized depletion of cladded layer evaporation because of higher heat energy input (Fig. 5d). The effect is shown clearly in the hardness values discussed in the later sections.

3.1.2 Microstructure and Morphology. Microstructure at the interface of the substrate and cladding layer plays a vital role in getting good bonding strength. In this investigation, variation in microstructural growth from base metal to cladding has been observed in the interface zone. Three distinct regions, namely clad layer, interface zone, and heat-affected zone, are observed in the cross-sectional images of the cladding samples prepared at 37.5 (Fig. 5a), 45 (Fig. 5b), 60 (Fig. 5c), 75 J/mm^2 (Fig. 5d) laser energy density. The diffusion of ZrO_2 into the substrate is higher in the case of higher laser energy density (i.e., in Fig. 5c, 60 J/mm^2). Some porosity but no crack is also observed in the samples having a higher clad thickness (i.e., in Fig. 5c, 60 J/mm^2); as the solubility of the gas increases with temperature, the dissolved gases are entrapped inside the molten pool, which results in porosity in the cladding. The appearance of pores may be due to the presence of entrapped

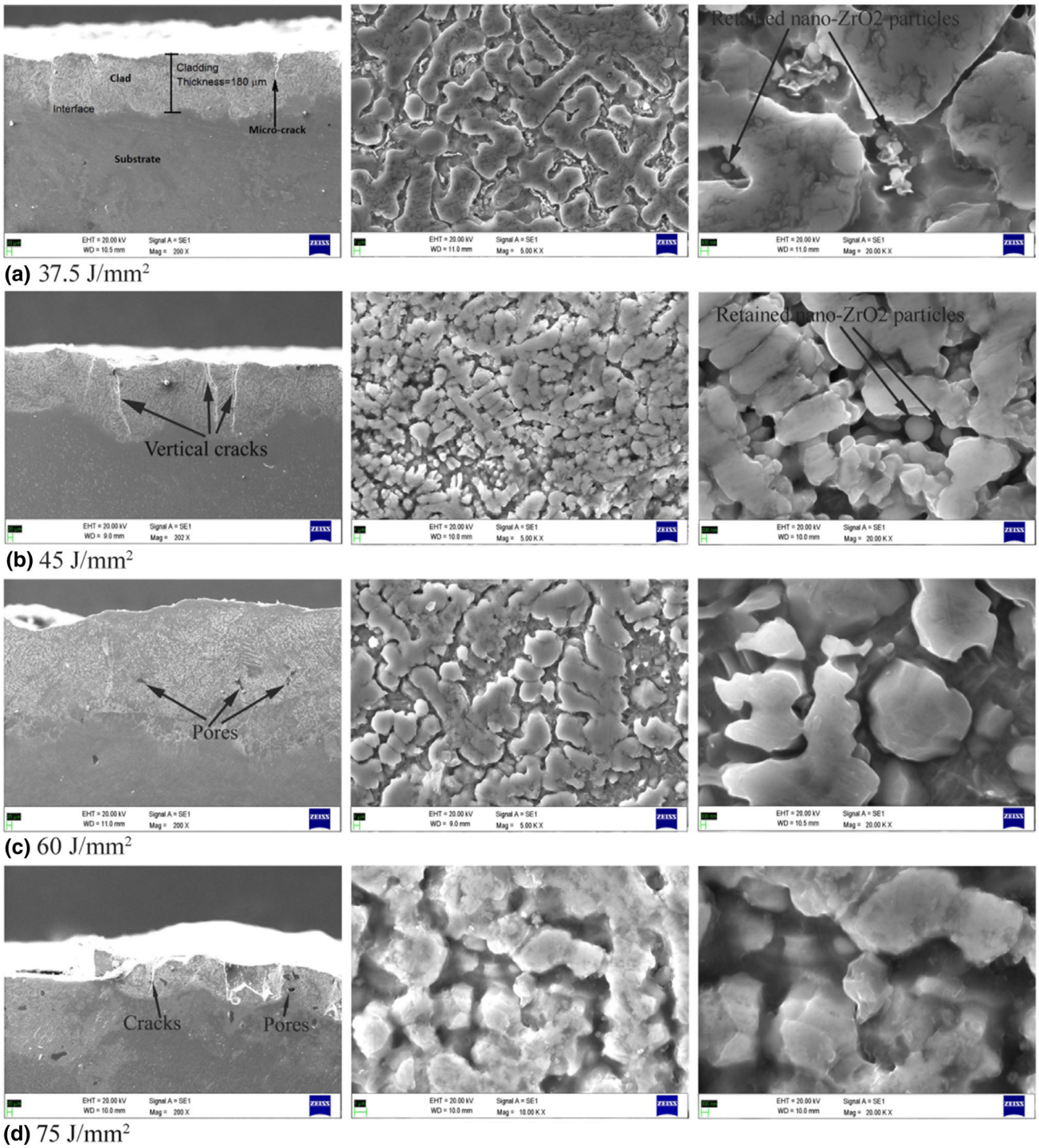

Fig. 5 Cross-sectional SEM images of composite cladding at different laser energy showing retention of agglomerated ZrO_2 in molten and re-solidified ZrO_2

and soluble gases inside the molten pool. The rejection of the soluble gases in the molten pool has taken place during solidification as the solubility decreases with the reduction in temperature. Moreover, the appearance of these voids may be augmented by the solidification shrinkage phenomenon, in places that are far away from the surface. The wettability of the cladding material with the substrate material is also an important property to be considered for strong metallurgical bonding. Microstructure at the interface is observed with a homogenous dispersion of the reinforced particles in the matrix, which confirms good wettability (Fig. 6a). From the cross-sectional EDS area mapping images at the interface (Fig. 6a), gradual microstructure change is observed which is responsible for graded change of property at the interface and it also ensures good mechanical interlocking against the peel force trying to uproot the coatings from the substrate. In the SEM images, the presence of the zirconia phase is visible in the form of a molten and partially molten state (Fig. 5a, b). From these

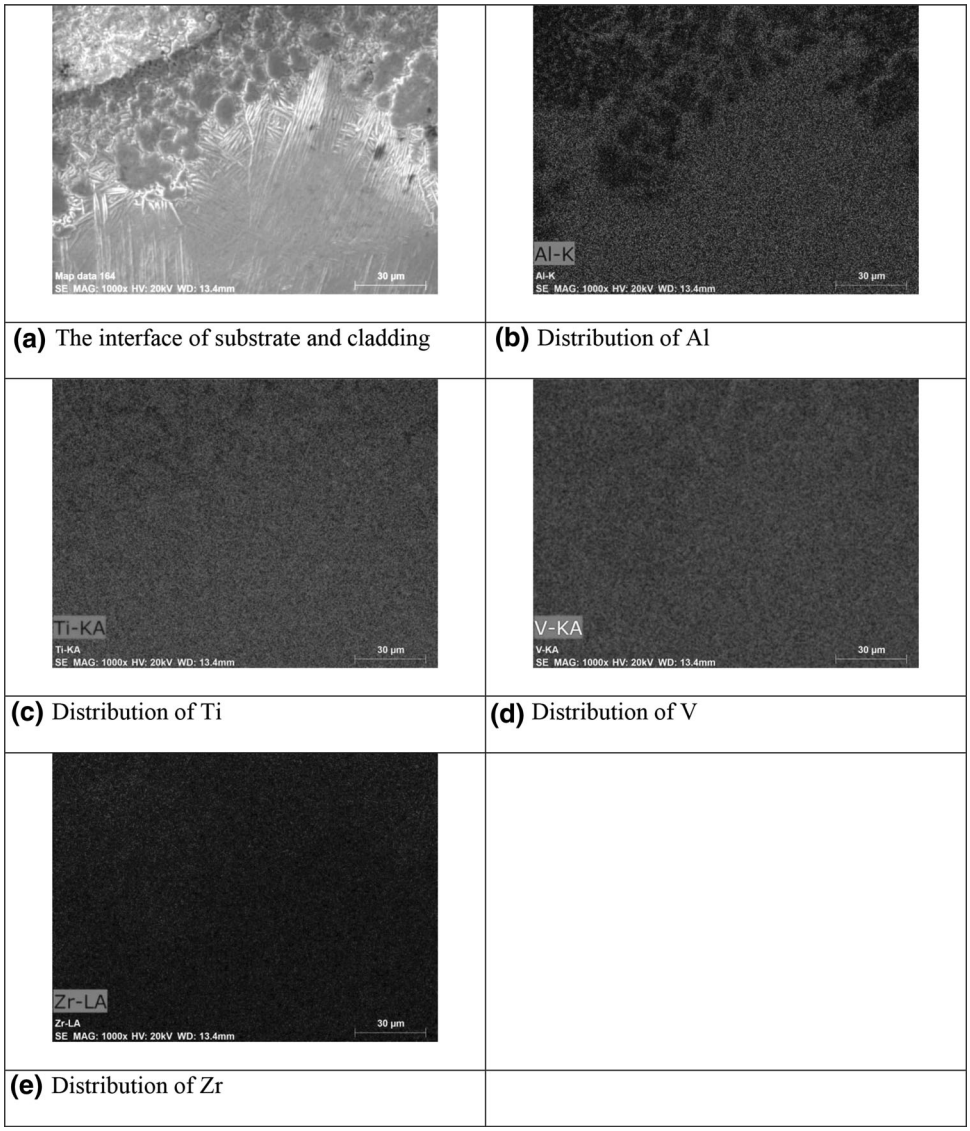

Fig. 6 Cross-sectional EDS area mapping of cladding at the interface showing the distribution of constituent elements

images, it can be observed that a uniform distribution of ZrO_2 powder as a reinforcement particle in the matrix of Ti6Al4V alloy has taken place.

3.1.3 Energy Dispersive Spectroscopy (EDS) Analysis. A scanning area of 80×50 µm was selected randomly at the interface of the substrate and the clad layer to investigate the distribution of the various chemical constituents such as titanium, aluminum, vanadium, and zirconium. The EDS area scan data of composite claddings are presented in Fig. 6. The presence of the above elements is observed in a gradient manner from the clad layer to the substrate. The concentration of ZrO_2 varies high to low from the top surface of the cladding layer toward the interface, whereas the concentration of other reinforced particles varies oppositely with the former. This may be due to the evaporation of the matrix and reinforcements (mainly Al_2O_3 and TiO_2, boiling point 2977, 2972 °C, respectively).

3.1.4 X-ray Diffraction Analysis. X-ray diffraction (XRD) patterns of the coatings taken at 45 and 60 J/mm^2 are presented in Fig. 7. It contains several peaks of TiO_2, Al_2O_3, and ZrO_2 phases. The Ti6Al4V alloy is composed of titanium, aluminum, and vanadium elements. Hence, the oxides formed in the cladding layer are TiO_2, Al_2O_3, and ZrO_2. (Titanium oxide is readily formed at 1200 °C. The titanium oxide is already in the molten state at 1843 °C before the melting of zirconia at 2715 °C. The formation of aluminum oxide might have taken place in the presence of atmospheric oxygen at this higher temperature.) These oxides may be formed due to the high temperature happening due to the irradiation of the laser beam. Zhuang et al. (Ref 18) deposited Ni-Ti-Si on Ti6Al4V alloy using the laser cladding method and found an oxidation film formed on the coating mainly consisting of TiO_2, Al_2O_3, etc. Several peaks of monoclinic, tetragonal, cubic, orthorhombic phases of ZrO_2 along with the peaks of TiO_2, Al_2O_3 are found in the XRD pattern of composite cladding in all samples prepared at all the laser energy level. The monoclinic phases can make the coating tougher because of the pressure-induced volume expansion phenomenon, while the cubic and tetragonal phases of ZrO_2 have better thermal barrier capability and high-temperature phase stability. From the XRD pattern, more

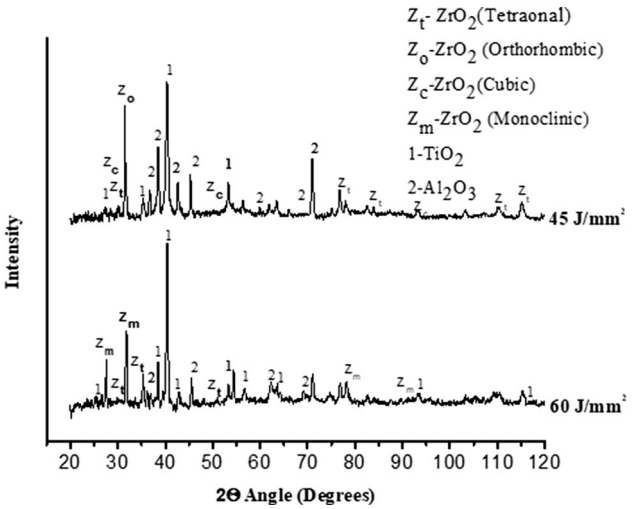

Fig. 7 XRD pattern of cladding samples prepared with 45 and 60 J/mm^2 laser energy

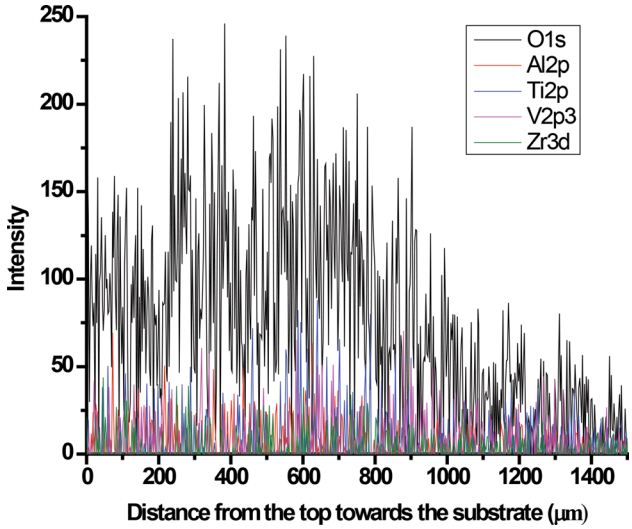

Fig. 8 XPS spectrum of cladding cross section showing the presence of Al, Zr, V, O, and Ti elements

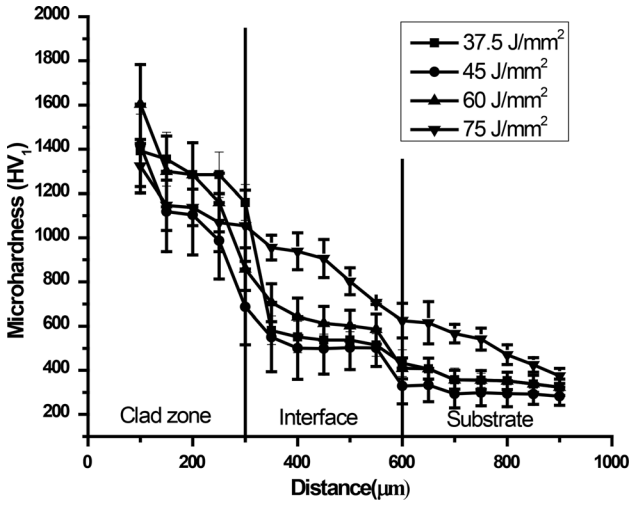

Fig. 9 Variation of microhardness from the clad layer to the substrate

number of cubic zirconia is observed with the energy input of 45 J/mm^2. Cubic zirconia has better high-temperature stability than other structures of zirconia owing to have a higher hardness of the cladding.

3.1.5 X-ray Photoelectron Spectroscopy (XPS) Analysis. Considering the presence of elements such as Zr, Ti, Al, V, and O in the cladding, XPS analyses were carried out for further confirmation of the elements. The XPS spectrum of the cladded sample (45 J/mm^2) showing the presence of Al, Zr, V, O, and Ti elements at different binding energy levels is shown in Fig. 8. The surface scanning of the sectioned sample shows the lower concentration of O1*s* peaks from the cladding top surface to the base material. The presence of peaks centered at 530.6, 532.7, and 535.1 eV correspond to oxygen involved in sub-oxides and oxide formation. The presence of ZrO_2 in the cladding can also be observed from the XPS spectrum of the cross section of the cladded sample (Fig. 8). The peak of Zr3*d* (183.6 eV), Al2*p* (74.1 eV), Ti2*p* (455 eV) along with the peaks of O1*s* is the characteristic of ZrO_2, Al_2O_3, and TiO_2 present in the cladding (Ref 19, 20). Similar peaks are also observed in the XPS spectrum in the scanning of the composite cladding samples after the wear test (Fig. 14).

3.2 Mechanical Properties of the Cladding

Microhardness is an important mechanical property to characterize the cladding surface. The microhardness testing was conducted at three different places, namely the clad layer, interface zone, and the substrate (Fig. 9). The average microhardness of samples prepared at 37.5, 45, 60, and 75 J/mm^2 laser energy density in the clad layer, interface zone, and the substrate is shown in Fig. 9. Higher hardness values are observed than the substrate, irrespective of the laser energy density. The enhancement of the microhardness may be due to the formation of a harder chemical compound such as TiO_2, Al_2O_3, and ZrO_2. The presence of these harder metallic oxides is evident from the x-ray diffraction analysis given in Fig. 7 and XPS analysis shown in Fig. 8. The average microhardness at the interface is also higher than the base metal maybe for two reasons: (1) martensitic structure formation due to the high-temperature gradient resulting in rapid solidification, and (2) because of the embedding of oxides as reinforcement in the matrix. But the average microhardness at the interface of the samples prepared at an energy input of 75 J/mm^2 compared to other energy inputs is lower than samples maybe due to higher interdendritic space. This may also be due to having comparatively lower cladding thickness resulting in higher heat transfer, relatively less temperature gradient (than the case of 60 J/mm^2), and higher hardness. More dilution of the harder compound in the matrix might have taken place while processing with higher energy input.

3.3 Wear Tests

The evaluation of the wear behavior of the cladded samples prepared at different laser energy density was carried out in a dry sliding pin-on-disk setup. The average weight loss of the cladded samples during the wear test is presented in Fig. 10. The plot indicates that the average weight losses of the samples are varying in the range of 0.012 to 0.55 g depending on the laser energy density for the same test conditions (i.e., distance

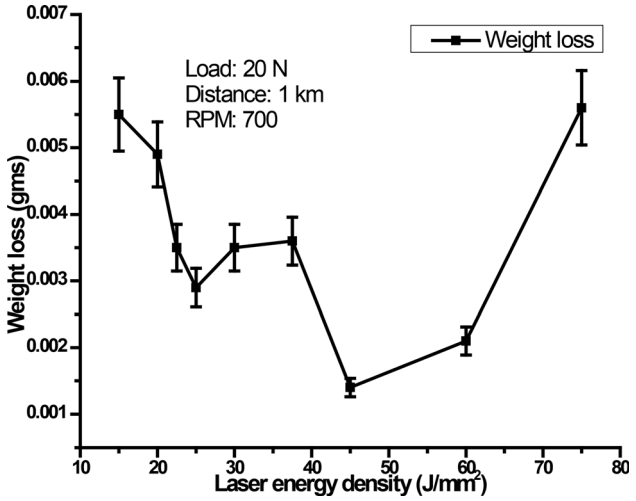

Fig. 10 Weight loss of cladding samples with the laser energy density

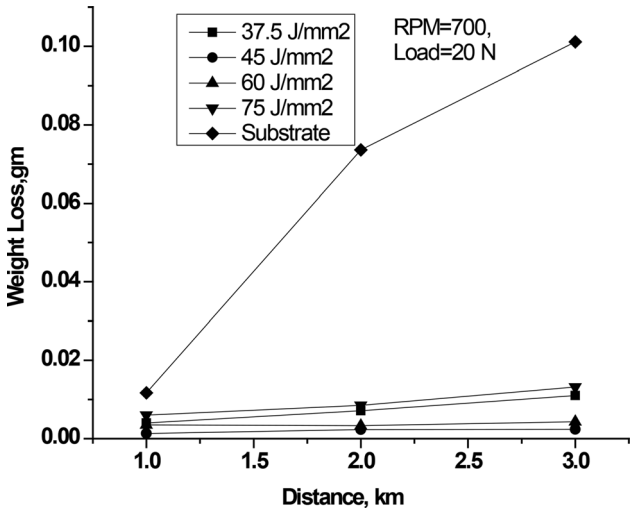

Fig. 11 Variation of weight loss of the cladding samples with distance

1 km, load 20 N, 700 rpm). Weight loss due to wearing gradually decreases with an increase in laser energy input up to 45 J/mm^2 and increases further with higher laser energy input. Weight loss due to wear is found to be minimum with a laser energy input of 45 J/mm^2 and higher in the cladded samples prepared in laser energy of 15, 22.5, 30 J/mm^2. As the wear in samples prepared with laser energy density of 15, 22.5, 30 J/mm^2 shows higher weight loss in the wear test, further wear tests with varying distance and magnitude of the applied load were conducted for samples prepared at 37.5, 45, 60, 75 J/mm^2. Figure 11 shows the variation of weight loss of samples made with 37.5, 45, 60, 75 J/mm^2 during wear test conducted for longer sliding distances and compared with the weight loss of the substrate in the same test conditions (load 20 N, 700 RPM, varying distance). The result shows the weight loss of the substrate is much higher than the cladded samples (0.1 g at 3 km), and samples prepared at laser energy density of 45 and 60 J/mm^2 have better wear performance in these test conditions. Thus, it is perceived that the wear resistance of the cladded samples is better than the substrate, for all these test distances (Fig. 11). Furthermore, from the plot (Fig. 12), it is also apparent that with the increase in applied normal load (from 10 to 30 N) during the wear test (conducted keeping the same sliding distance and speed), the weight loss of the cladded samples increases steadily in all the samples prepared with laser energy of 37.5, 45, 60, 75 J/mm^2. Higher weight losses are observed on increasing the load due to the higher value of the stress. As the hardness values of the cladded samples are reasonably higher than the Ti-6Al-4V substrate (due to in situ formed oxide phases such as Al_2O_3, TiO_2 along with the reinforced ZrO_2 in the clad layer), it restricts the sliding wear and lessens the weight loss of the cladded samples. From the microstructural analysis and assessment of microhardness values, it was evident that the harder and denser phases are found in the samples prepared at 45 and 60 J/mm^2 which is the reason for lower weight loss in these samples. The optical micrographs of worn-out surfaces of the substrate Fig. 13(a) and samples prepared at 30, 37.5, 45, 60, 75 J/mm^2 are shown in Fig. 13(a)-(f). The wear mechanism in the substrate is primarily due to abrasion and plowing in the substrate being softer (Fig. 13a), whereas the wear mechanism of the cladded samples is due to abrasion and removal of the cladded oxides materials. Worn-out surface of the cladded samples (30 and 37.5 J/mm^2) are nonuniform, whereas more uniform wear has taken place in the samples prepared at 45 and 60 J/mm^2 (Fig. 13d and 14d). Figure 13(f) shows a worn surface containing more of Ti6Al4V powder than the ZrO_2. This may be due to the combined effect of evaporation, higher dilution resulting in a change in the proportion of the ZrO_2, Al_2O_3, TiO_2 (Fig. 13f) in the substrate, and during the wear test the harder phases are uprooted from the softer matrix (Ti6Al4V). This shows a higher weight loss of the samples prepared at this (75 J/mm^2) level of laser energy density. XPS spectra of the cross section of the cladded samples done at different laser energy density after wear test are presented in Fig. 14. It shows the presence of Zr, Al, Ti, V, O elements even after wear. The line scanning of the sectioned sample shows the lower concentration of O1*s* peaks from the cladding top surface to the base material. The presence of peaks centered at a binding energy of 530.6, 532.7, and 535.1 eV corresponds to oxygen involved on sub-oxides and oxide formation. The presence of Zr3*d* (183.6 eV), Al2*p* (74.1 eV), Ti2*p* (455 eV) peaks along with peaks of O1*s* is the characteristic of ZrO_2, Al_2O_3, and TiO_2 present in the cladding as reported by Madeira et al. (Ref 19) and Muhaffel et al. (Ref 20). The presence of ZrO_2 in the cladding can also be observed from the XPS spectrum of the cross section of the cladded sample (Fig. 14). Similar peaks are also observed in the XPS spectrum in the surface scanning of the composite cladding samples (Fig. 8). Hence, with proper control of the laser parameters (scanning speed, spot diameter, overlapping, laser power, etc.), it could be possible to produce a wear-resistant coating with a reduced coefficient of friction. The coefficient of frictions as a function of time for claddings and substrate material is shown in Fig. 15. These are obtained from the dry sliding wear test conducted at room temperature. The coefficient of friction is lying in the range of 0.25-0.38 for all the samples, whereas the substrate material has a higher coefficient of friction (0.45 approximately, Fig. 15). At beginning of the wear test, loosely bonded ZrO_2 from the cladded sample peels due to sliding against the rotating plate

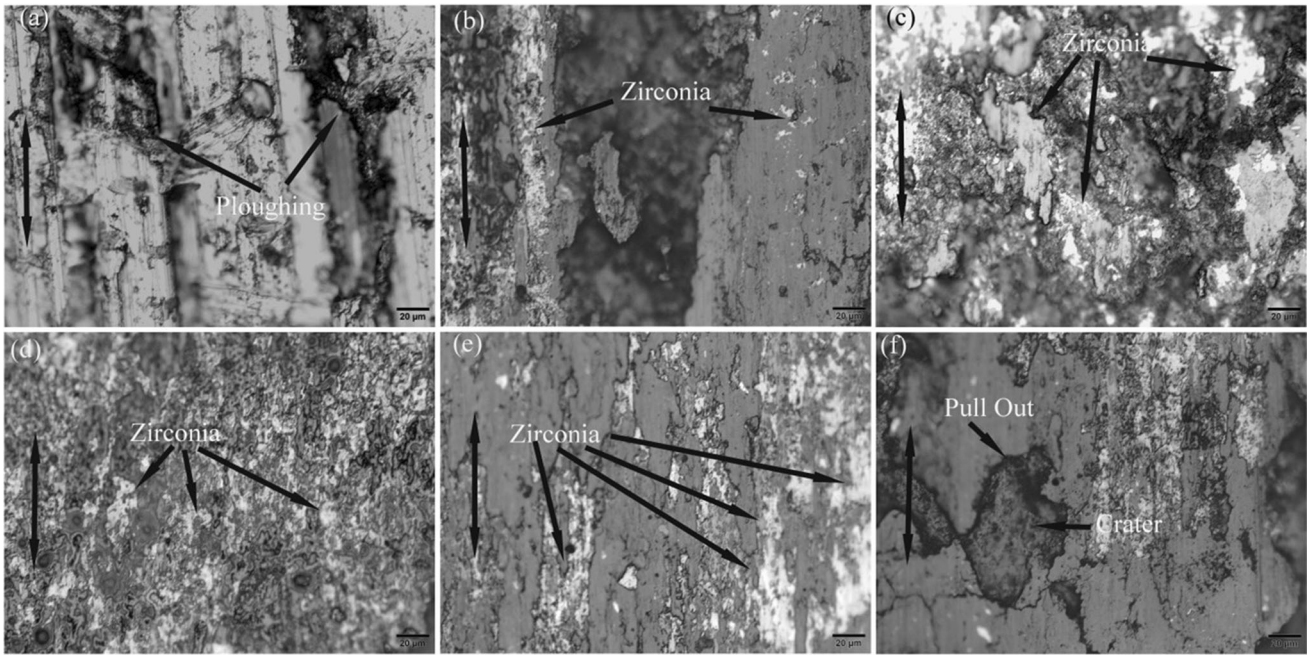

Fig. 12 Variation of weight loss of the cladding samples with load

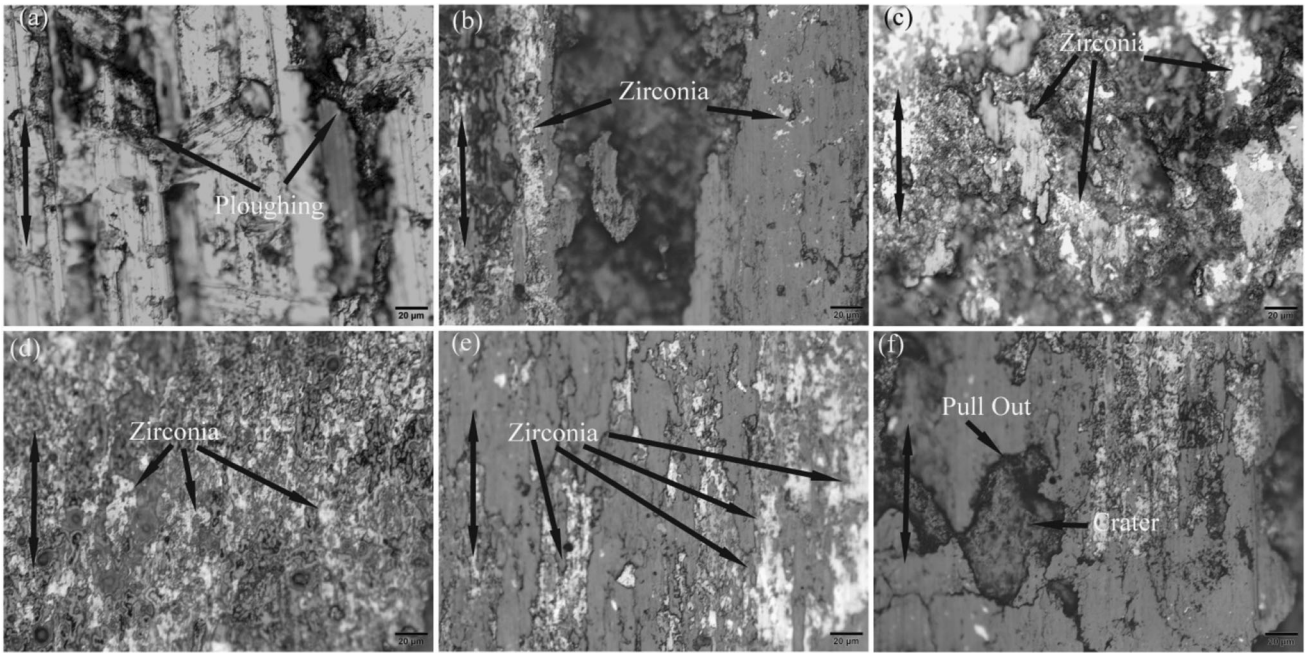

Fig. 13 Optical micrographs of worn-out surfaces (a) substrate, (b) cladded sample with 30 J/mm^2, (c) cladded sample with 37.5 J/mm^2, (d) cladded sample with 45 J/mm^2 (e) cladded sample with 60 J/mm^2, (f) cladded sample with 75 J/mm^2

under load. Then, the protruded portion of the nonuniform coating surface uprooted due to high contact stresses. This phenomenon is observed in the plot showing a high coefficient of friction in the initial period. Relatively, a uniform variation of coefficient of friction is observed thereafter. The coated sample at 37.5 and 45 J/mm^2 shows a lower coefficient of friction than other samples (Fig. 15). This can be seen from the optical micrographs of worn-out surfaces (Fig. 14c and d).

4. Conclusions

Surface modification of the Ti6Al4V substrate was conducted by the preplacement of composite powder (Ti6Al4V and nano-ZrO_2 powder) using laser energy. The composite claddings of Ti6Al4V (wt. 80%)-nano-ZrO_2 (wt. 20%) were deposited on a Ti6Al4V substrate surface. The salient observations are summarized as follows:

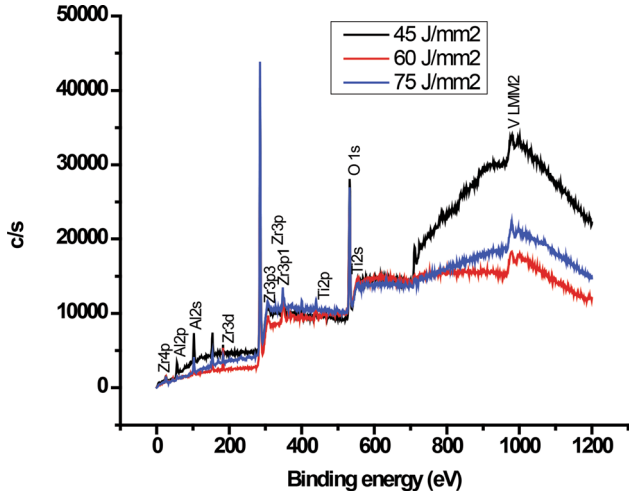

Fig. 14 XPS spectra of cladding surface done at different laser energy density after wear test showing the presence of Zr, Al, Ti, V, O elements

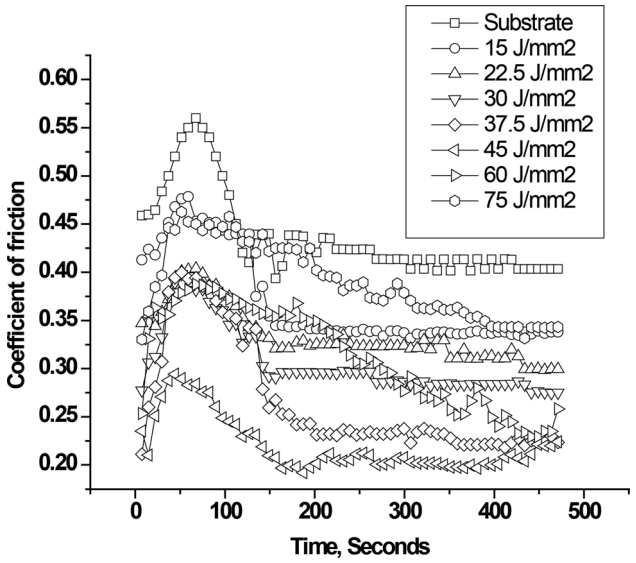

Fig. 15 Friction coefficient as a function of time for different claddings and substrate

Overlay coating of ZrO_2 using laser irradiation is difficult as it transmits about 70% and reflects about 25% of the incident laser ray. But in the present research, ZrO_2 cladding has been done as melting and solidification of composite powders have taken place in the molten pool of Ti6Al4V, TiO_2, Al_2O_3, etc. The cladding layer thickness obtained in this process is in the range of 0.25-0.6 mm. The reduction in the cladding thickness may be due to the evaporation of the elements with a relatively lower boiling point at the higher laser energy level. Due to the rapid and non-equilibrium solidification process, the solubility of atmospheric gases in the molten pool, some pores, and vertical cracks is observed in the cladding layer. However, the occurrence of these cracks and pores can be avoided by selecting suitable laser parameters and the weight percentage of the composite powders (i.e., in the range of lased energy density of 45 and 60 J/mm^2). Reactive laser sintering between Ti6Al4V and ZrO_2 particles resulted in the synthesis of hard and wear-resistant metallic oxides like TiO_2, $Al2O_3$, ZrO_2, etc. These oxides get embedded in the molten pool of the base metal up to few micron depths ensuring good adhesion to the substrate. They also form a solid solution with each other. The resulted reaction products act as reinforcement and have good wettability in the matrix. Hence, the composite cladding improves surface hardness (3-4 times) and wear resistance properties.

References

1. H. Zhou, F. Li, B. He, J. Wang and B. de Sun, Air Plasma Sprayed Thermal Barrier Coatings on Titanium Alloy Substrates, *Surf. Coat. Technol.*, 2007, **201**(16–17), p 7360–7367
2. V. Koshuro, A. Fomin and I. Rodionov, Composition , Structure and Mechanical Properties of Metal Oxide Coatings Produced on Titanium Using Plasma Spraying and Modi Fi Ed by Micro-Arc Oxidation, *Ceram. Int.*, 2018, **44**(11), p 12593–12599. https://doi.org/10.1016/j.ceramint.2018.04.056
3. K.S. Selivanov, A.M. Smyslov, Y.M. Dyblenko and I.P. Semenova, Erosive Wear Behavior of Ti/Ti(V, Zr)N Multilayered PVD Coatings for Ti-6Al-4V Alloy, *Wear*, 2019, **419**, p 160–166
4. P. Wiecinski, J. Smolik, H. Garbacz, J. Bonarski, A. Mazurkiewicz and K.J. Kurzydłowski, Microstructure and Properties of Metal/Ceramic and Ceramic/Ceramic Multilayer Coatings on Titanium Alloy Ti6Al4V, *Surf. Coatings Technol.*, 2017, **309**, p 709–718
5. R. Sitek, J. Kaminski, J. Borysiuk, H. Matysiak, K. Kubiak and K.J. Kurzydlowski, Microstructure and Properties of Titanium Aluminides on Ti6Al4V Titanium Alloy Produced by Chemical Vapor Deposition Method, *Intermetallics*, 2013, **36**, p 36–44
6. G. Xu and X. Shen, Fabrication of SiO2 Nanoparticles Incorporated Coating Onto Titanium Substrates by the Micro Arc Oxidation to Improve the Wear Resistance, *Surf. Coat. Technol.*, 2019, **364**, p 180–186
7. B.A. Obadele, A. Andrews, P.A. Olubambi, M.T. Mathew and S. Pityana, Effect of ZrO2 Addition on the Dry Sliding Wear Behavior of Laser Clad Ti6Al4V Alloy, *Wear*, 2015, **328–329**, p 295–300. https://doi.org/10.1016/j.wear.2015.02.056
8. C. Xia, Z. Zhang, Z. Feng, B. Pan, X. Zhang, M. Ma and R. Liu, Effect of Zirconium Content on the Microstructure and Corrosion Behavior of Ti-6Al-4V-XZr Alloys, *Corros. Sci.*, 2016, **112**, p 687–695. https://doi.org/10.1016/j.corsci.2016.09.012
9. Y. Liu, W. Liu, Y. Ma, C. Liang, C. Liu, C. Zhang and Q. Cai, Microstructure and Wear Resistance of Compositionally Graded Ti–Al Intermetallic Coating on Ti6Al4V Alloy Fabricated by Laser Powder Deposition, *Surf. Coatings Technol.*, 2018, **353**, p 32–40. https://doi.org/10.1016/j.surfcoat.2018.08.067
10. S. Kumar, A. Mandal, A.K. Das and A.R. Dixit, Parametric Study and Characterization of AlN-Ni-Ti6Al4V Composite Cladding on Titanium Alloy, *Surf. Coat. Technol.*, 2018, **349**, p 37–49
11. M.L. Lepule, B.A. Obadele, A. Andrews and P.A. Olubambi, Corrosion and Wear Behaviour of ZrO2 Modified NiTi Coatings on AISI 316 Stainless Steel, *Surf. Coat. Technol.*, 2015, **261**, p 21–27
12. G. Ma, S. Yan, D. Wu, Q. Miao, M. Liu and F. Niu, Microstructure Evolution and Mechanical Properties of Ultrasonic Assisted Laser Clad Yttria Stabilized Zirconia Coating, *Ceram. Int.*, 2017, **43**(13), p 9622–9629
13. I. Yamashita, M. Kudo and K. Tsukuma, Development of Highly Transparent Zirconia Ceramics, *12 TOSOH Res. Technol.*, 2012, **56**(201), p 11–16
14. J. Wilkes, Y. Hagedorn, W. Meiners and K. Wissenbach, Additive Manufacturing of ZrO2-Al_2O_3 ceramic components by selective laser melting, *Rapid Prototyping J.*, 2013, **1**, p 51–57
15. A. Hattal, T. Chauveau, M. Djemai, J.J. Fouchet, B. Bacroix and G. Dirras, Effect of Nano-Yttria Stabilized Zirconia Addition on the Microstructure and Mechanical Properties of Ti6Al4V Parts Manufactured by Selective Laser Melting, *Mater. Des.*, 2019, **180**, p 107909. https://doi.org/10.1016/j.matdes.2019.107909
16. T.A. Schaedler, O. Fabrichnaya and C.G. Levi, Phase Equilibria in the TiO2-YO1.5-ZrO2 System, *J. Eur. Ceram. Soc.*, 2008, **28**(13), p 2509–2520
17. R. Chakraborty, M.S. Raza, S. Datta and P. Saha, Synthesis and Characterization of Nickel Free Titanium-Hydroxyapatite Composite

Coating over Nitinol Surface Through In-Situ Laser Cladding and Alloying, *Surf. Coatings Technol.*, 2018, **358**, p 539–550. https://doi.org/10.1016/j.surfcoat.2018.11.036

18. Q. Zhuang, P. Zhang, M. Li, H. Yan and Z. Yu, Microstructure, Wear Resistance and Oxidation Behavior of Ni-Ti-Si Coatings Fabricated on Ti6Al4V by Laser Cladding. *Materials*, 2017, **10**(11), p 1248. https://doi.org/10.3390/ma10111248
19. S. Madeira, A.M.P. Pinto, L.C. Rodrigues, O. Carvalho, G. Miranda, R.L. Reis, J. Caramês and F.S. Silva, Effect of Sintering Pressure on Microstructure and Mechanical Properties of Hot-Pressed Ti6Al4V-ZrO2 Materials, *Mater. Des.*, 2017, **120**, p 394–403. https://doi.org/10.1016/j.matdes.2017.02.038
20. F. Muhaffel, M. Kaba, G. Cempura, B. Derin, A. Kruk, E. Atar and H. Cimenoglu, Influence of Alumina and Zirconia Incorporations on the Structure and Wear Resistance of Titania-Based MAO Coatings, *Surf. Coat. echnol.*, 2019, **377**, p 124900